Magnetic Properties

DOI: 10.1002/anie.200604236

A Low-Dimensional Iron(II) Phosphate Exhibiting Field-Dependent Magnetization Steps**

Wendy L. Queen, Shiou-Jyh Hwu, and Lei Wang*

Ferromagnetic materials often exhibit an enhanced magnetization response to an applied magnetic field when the magnetic ions are brought within close proximity of one another, that is, in a certain dimension or geometry. Common permanent magnets have a high saturation magnetization, coercive field, and remnant magnetization in hysteresis loops. Ferromagnetic solids exhibiting nearly rectangular hysteresis loops with a relatively small coercive field are suitable for magnetic recording and information-storage applications in computing. Ferro- and ferrimagnetic nanoparticles, which are currently used in information storage, become single-domain magnetic particles when their size is reduced below a critical value (less than 100 nm). In this regime, they can exhibit paramagnetic behavior below the Curie temperature (T_C), a phenomenon known as superparamagnetism. The onset of superparamagnetism places a limit on the storage density of future hard drives, as a result of the minimum size of particles that can be used. For the next generation of devices for quantum computing[1] and information storage,[2] ferro- and ferrimagnetic solids with confined magnetic lattices are sought because of the inherent quantum-mechanical effects associated with them.

We have begun to explore new extended solids containing electronically confined magnetic nanostructures.[3] Herein, we report $RbNa_3Fe_7(PO_4)_6$ (**1**), the first example of an iron(II) phosphate that exhibits field-dependent magnetization steps. Steps resulting from quantum tunneling of the magnetization have been reported for molecular magnets[4,5] and a few condensed solids, including the "spin-ice" pyrochlores (for example, $Dy_2Ti_2O_7$ and $Ho_2Ti_2O_7$)[6] and $Ca_3Co_2O_6$.[7] These compounds feature a large-spin ground state and significant magnetoanisotropy, which are essential properties for quantum-device applications. These features can be attributed to geometrically frustrated magnetic lattices[8] and to ions with uniaxial magnetic properties,[9] respectively. Other steplike anomalies in the magnetization of extended solids have been attributed to avalanches,[10a] spin rearrangements,[10b] and domain-wall depinning.[10c] Herein we report the structure and magnetic properties of **1**, in light of the detection of unusual field-dependent magnetization steps.

Compound **1** is a representative member of the large family of compounds $ANa_3M_7(PO_4)_6$ (A = K, Rb, Cs; M = Mn, Fe, Co; Table S1 in the Supporting Information). Light brown crystals of **1** were synthesized using high-temperature methods in a molten-salt medium. The crystal structure reveals a three-dimensional framework consisting of five unique FeO_n polyhedra ($n = 4+2$, 5, $5+1$, 6; the second numbers represent the number of long bonds) in each asymmetric unit (Supporting Information, Figures S1 and S2). For simplicity, the iron–oxygen network is viewed as iron–oxygen chains, which are interconnected by the $Fe(5)O_4$ polyhedra (Figure 1a) and the PO_4 units (Figure 1b). The nearest-neighbor magnetic couplings between iron(II) centers arranged in triangles bridged by oxygen atoms are highlighted in Figure 1a. Electronically, the PO_4 groups serve to space and possibly to insulate the magnetic iron–oxygen chains (Figure 1b).

In the overall structure, the chains of vertex-sharing FeO_n polyhedra, which run along the *a* direction, are connected into slabs parallel to the *ab* plane (Figure S3). The chains consist of trinuclear units of Fe(1)/Fe(2)/Fe(4) or Fe(2)/Fe(3)/Fe(4). The shorter Fe–O distances range from 2.01–2.26 Å and are comparable to the sum of the Shannon crystal radii of Fe^{2+} (0.92 Å) and O^{2-} (1.21 Å) of 2.13 Å.[11] The Fe-O-Fe bond angles range from 108.0–128.1° and are comparable to the values commonly reported for iron phosphates.[12] As expected, the Fe···Fe distance between the edge-sharing $Fe(1)O_6$ and $Fe(3)O_6$ polyhedra (3.215(1) Å) is shorter than those between the vertex-sharing polyhedra (3.38–3.88 Å). The Fe-O-Fe angle through the shared edge (99.76(1)°) is also smaller than those through the shared vertices. Given the diversity of bond distances and angles, multiple superexchange pathways and, thus, complex magnetic interactions are expected.

The DC magnetic susceptibility (χ) of a ground powder of selected crystals of **1** was measured as a function of temperature at applied magnetic fields (H) of 100 and 5000 Oe. Figure 2 shows the temperature dependence of the magnetization (M) of **1** at 100 Oe. The low-temperature region of the curve is compared to those of $KNa_3Fe_7(PO_4)_6$ and $CsNa_3Fe_7(PO_4)_6$ in the inset. The inverse of the molar magnetic susceptibility of **1** is linear as a function of temperature over 50–300 K at 100 Oe (Figure S4). A Curie–Weiss fit to the linear portion of the curve indicates an effective magnetic moment (μ_{eff}) of 5.2(9) μ_B, which is slightly higher than the

[*] W. L. Queen, Dr. S.-J. Hwu, L. Wang
Department of Chemistry
Clemson University
Clemson, SC 29634-0973 (USA)
Fax: (+1) 864-656-6613
E-mail: shwu@clemson.edu

[**] This work was supported by the National Science Foundation (DMR-0322905). Funds from the NSF for the purchase of a SQUID magnetometer (CHE-9808044) and of an X-ray diffractometer (ESR-9108772, CHE-9207230, 9808165) are also gratefully acknowledged. The authors are indebted to Dr. Jim O'Brien of Quantum Design for his assistance in fine-tuning the AC susceptibility measurement of Figure 5.

Supporting information for this article is available on the WWW under http://www.angewandte.org or from the author.

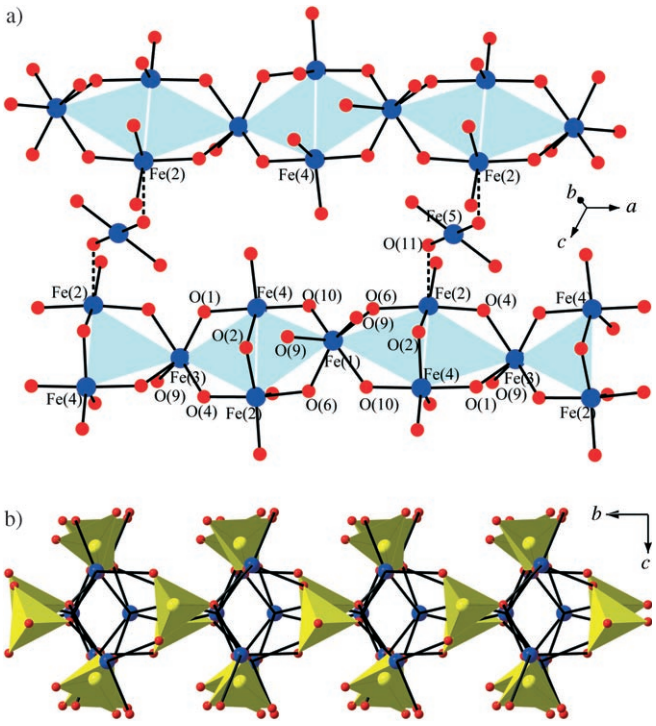

Figure 1. Fragments of the crystal structure of **1**. a) The iron–oxygen chains are interconnected through the Fe(5)O_4 polyhedra. The O(11) atoms of these polyhedra are shared with Fe(2) of the chains through long bonds of 2.48(1) Å (dashed). b) The iron–oxygen chains are also interconnected through the PO_4 tetrahedra. Fe blue, P yellow, O red; Rb and Na omitted for clarity. The triangular units of the magnetic lattices are highlighted in cyan. The Fe—O bonds of 2.01–2.26 Å are drawn in thick black lines. Selected interatomic distances [Å] and angles [°]: Fe(1)···Fe(2) 3.88(3), Fe(1)···Fe(4) 3.78(5), Fe(2)···Fe(3) 3.86(6), Fe(2)···Fe(4) 3.38(5), Fe(3)···Fe(4) 3.75(3); Fe(3)-O(1)-Fe(4) 125.5(1), Fe(2)-O(2)-Fe(4) 108.0(1), Fe(2)-O(4)-Fe(3) 128.1(1), Fe(1)-O(6)-Fe(2) 126.0(1), Fe(4)-O(10)-Fe(1) 127.1(1), O(4)-Fe(2)-O(6) 173.2(1), O(1)-Fe(4)-O(10) 177.3(1).

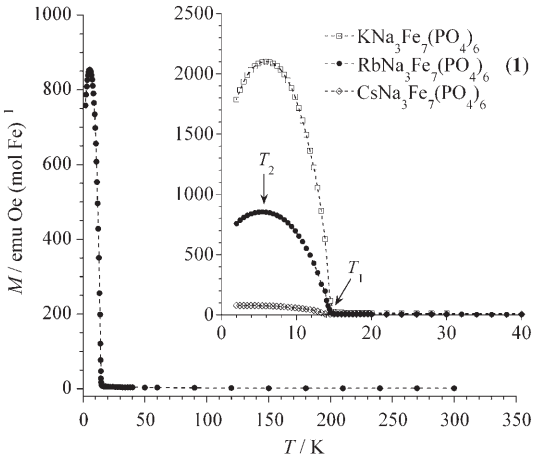

Figure 2. Temperature dependence of the magnetization of a powder sample of **1** at 100 Oe. Inset: The low-temperature region of the curve of **1** is compared to those of $KNa_3Fe_7(PO_4)_6$ and $CsNa_3Fe_7(PO_4)_6$. The data were collected as the samples were cooled in the applied field. The connecting dashed lines are to aid viewing.

spin-only moment of 4.9 μ_B expected for a high-spin Fe^{2+} (d^6) ion. As found for other highly correlated high-spin Fe^{2+} systems, we expect that the orbital contributions of the ligand field play a significant role,[13] causing the difference in the measured and expected values of the effective magnetic moments. The negative Weiss constant (θ) of −46(4) K, indicates an antiferromagnetic coupling of the nearest neighbors, which is consistent with the geometrically frustrated magnetic lattice highlighted in Figure 1 a.

The general features of the magnetization versus temperature curve of **1** at 100 Oe suggest a ferromagnetic transition at 14.6 K (T_1) followed by a ferro-to-antiferromagnetic transition at 6 K (T_2). The second transition is suppressed at higher fields (for example, at 5000 Oe; Supporting Information Figure S5). The magnetization versus temperature curves of the $ANa_3Fe_7(PO_4)_6$ series show a systematic decrease in the magnitude of the magnetization below T_1 with increasing size of the A-site cation. The large ferromagnetic moment of the compounds is due to the exchange field (Weiss field) of the closely spaced magnetic Fe^{2+} ions.[14] The magnetization values near T_2 increase when the magnetic ions are brought closer together upon replacement of the Rb^+ ions with smaller K^+ ions. The general profile of the magnetization versus temperature curves suggests predominately antiferromagnetic coupling above T_1. Between T_1 and T_2, ferromagnetic interactions dominate, overcoming the decrease in the magnetic moment. The drop in the moment below T_2 could signal an additional antiferromagnetic coupling or zero-field splitting.

The field-dependent magnetization measurements confirm the ferrimagnetic ordering, as well as the presence of uniaxial magnetic properties. The experiments were carried out on an oriented single crystal of **1** (0.3 mg). The hysteresis curves of relative magnetization (M/M_s; M_s is the saturation magnetization at 5×10^4 Oe) versus field were acquired with the magnetic field applied along the crystallographic *a* axis (Figure 3), which is approximately parallel to the pseudo-threefold rotation axes of the distorted Fe(2)O_5 and Fe(4)O_5 trigonal bipyramids (Figure 1). The magnetization versus field curves measured immediately below T_1, at 10 and 12 K, confirm the existence of ferromagnetic coupling. At temperatures below T_2, steps occur in the hysteresis loops. The steep increase in magnetization at each step may indicate field-induced metamagnetism, which could possibly be attributed to one of the following structural characteristics or combinations thereof: geometrically frustrated triangles in the magnetic lattice (Figure 1, left), the short Fe···Fe distance between the edge-sharing Fe(1)O_6 and Fe(3)O_6 polyhedra, or the uniaxial properties of the Fe^{2+} moments of the Fe(2)O_5 and Fe(4)O_5 trigonal bipyramids. Note that these step transitions are much sharper for the single crystal than for the polycrystalline sample first investigated (Supporting Information Figure S6), indicating a large magnetic anisotropy. Furthermore, the hysteresis is diminished when the magnetic field is applied along directions orthogonal to the crystallographic *a* axis (Supporting Information Figure S7).

Zero-field-cooled (ZFC) and field-cooled (FC) measurements of the magnetic moment were carried out on the oriented single crystal over a temperature range including the

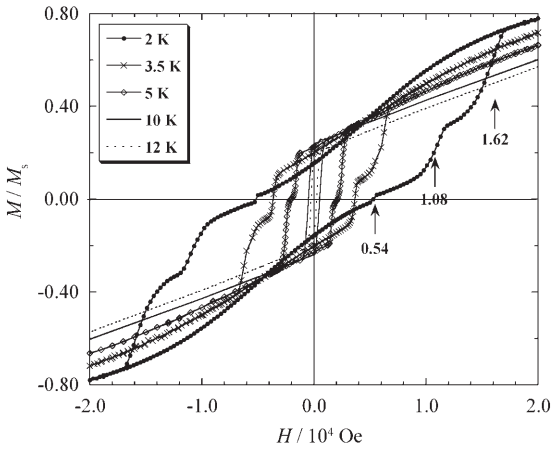

Figure 3. Magnetization versus magnetic field (applied along the *a* axis) hysteresis loops of a single crystal of **1** at 2–12 K. The magnetization is normalized to its saturation value at 5×10^4 Oe. For the curve at 2 K, the steps occur at regular field intervals of approximately 5.4×10^3 Oe. See text for details. The connecting lines are to aid viewing.

transitions at applied fields of 1, 50, 250, and 1000 Oe (Figure 4). A strong easy-axis anisotropy was quantified ($M_a/M_\perp \approx 1330$ at 7 K and 1 Oe), and the second transition

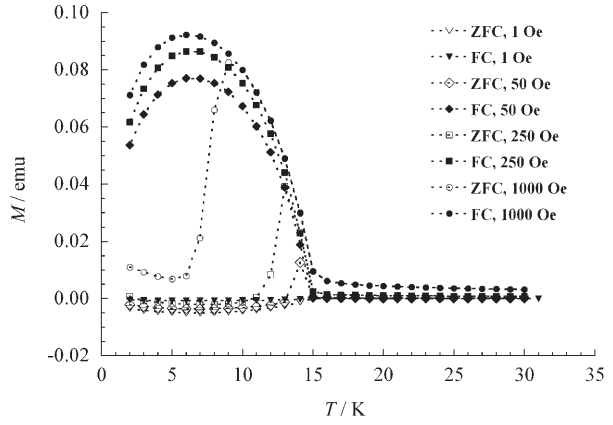

Figure 4. Temperature dependence of the magnetic moment of a single crystal of **1**, measured under ZFC and FC conditions at different magnetic fields (applied along the *a* axis). The connecting dashed lines are to aid viewing.

was found to occur below the merging temperature of the ZFC and FC curves. The temperature at which the plots merge decreases as the applied field increases, which is consistent with the notion of a field-induced transition or spin flipping due to magnetic frustration, while T_2 conceivably remains unchanged in the FC curves. The magnetic tail in the ZFC curves suggests that these transitions are the result of field-induced spin coupling.

Further evidence provided by AC susceptibility measurements also suggests an intriguing change in the spin dynamics around T_1. Figure 5 shows the temperature dependence of the real component of the AC magnetic susceptibility (χ') of a single crystal of **1** at five different frequencies at zero field. A

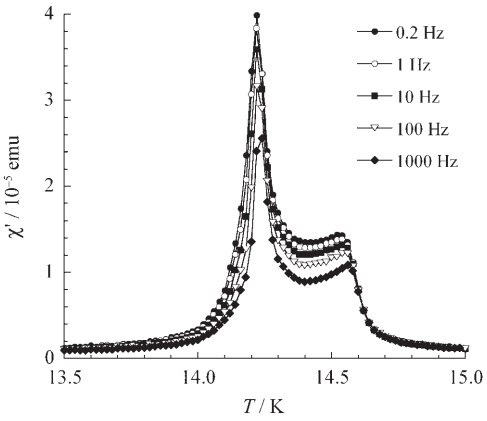

Figure 5. Temperature dependence of the real component of the AC magnetic susceptibility of a single crystal of **1** at different frequencies at zero field. The connecting lines are to aid viewing.

double-peak feature is detected, which corresponds to the shoulder near T_1 (Supporting Information Figure S5). As the frequency is increased, the susceptibility decreases. For temperatures below T_1, hysteresis appears in the magnetization versus field curves (Figure 3); the curve at 2 K exhibits a succession of magnetization steps with a roughly constant field spacing of approximately 5.4×10^3 Oe. The AC susceptibility measurements, however, do not provide evidence of the temperature shift of the transitions (data not shown) necessary for quantum tunneling of the magnetization.[15] Thus, we feel that spin frustration probably underpins the field-dependent jumps in the magnetization observed in Figure 3.

Finally, the new family of compounds $ANa_3M_7(PO_4)_6$, of which **1** is a member, presents the opportunity to systematically investigate the field-dependent magnetization steps. Knowing that the magnetic behavior in condensed phases is sensitive to the local structure, where magnetic spins are coupled, we plan to study the correlation between the structures and properties of the compounds listed in Table S1. Preliminary heat-capacity studies reveal a small change in the latent heat at T_1, which is indicative of a transition that is electronic in nature. To shed new light on the origin of the magnetic anomalies, field-dependent heat-capacity measurements and neutron-scattering studies are in order. Geometrically induced magnetic frustration, as stated above, can lead to non-zero magnetic spin and to magnetic anomalies in field- and temperature-dependent magnetization processes.[1] We will also carry out torque measurements and theoretical calculations to investigate the uniaxial magnetic properties of the high-spin Fe^{2+} (d^6) ions in the trigonal bipyramidal sites. We anticipate the discovery of more fascinating compounds containing magnetic nanostructures, especially compounds possessing large numbers of magnetic spins.

Experimental Section

1: FeO (0.251 g) and P_4O_{10} (0.1066 g) were ground in a RbCl/NaCl flux (ca. 0.5 g) and placed in a carbon-coated fused-silica ampoule, which was sealed under vacuum. The ampoule was heated to 700 °C

and held at this temperature for 4 days. Then it was slowly cooled to 450 °C and finally cooled to room temperature. The yield of **1** was approximately 20%, and the by-products were $(RbCl)Na_2Fe_3(P_2O_7)_2$[16a] and $NaFe_{3.67}(PO_4)_3$.[16b]

Crystal data for **1**: $RbNa_3Fe_7(PO_4)_6$, $M_r = 1115.2$, monoclinic, space group $C2/c$ (no. 15), $a = 12.981(3)$, $b = 10.777(2)$, $c = 15.732(3)$ Å, $\beta = 113.62(3)°$, $V = 2016(3)$ Å^3, $Z = 4$, $\rho_{calcd} = 3.673$ g cm^{-3}, $Mo_{K\alpha}$ ($\lambda = 0.71073$ Å) radiation, $2.50 < 2\theta < 52.5°$, final $R = 0.0276$, $Rw = 0.0824$, GOF = 0.989 (all data), 191 parameters. Data were collected on a four-circle Rigaku AFC8 diffractometer equipped with a Mercury CCD area detector. Compound **1** is isostructural with $CsNa_3Zn_7(PO_4)_6$.[17] Further details on the crystal structure investigation may be obtained from the Fachinformationszentrum Karlsruhe, 76344 Eggenstein-Leopoldshafen, Germany (fax: (+49) 7247-808-666; e-mail: crysdata@fiz-karlsruhe.de), on quoting the depository number CSD-417109.

Magnetic measurements: Magnetic susceptibility was measured with a Quantum Design SQUID MPMS-5S magnetometer. A ground powder of selected single crystals (9.9 mg) was placed in a gel capsule. The initial temperature-dependent studies were performed over 2–300 K in applied fields of 100 and 5000 Oe. The magnetic susceptibility was corrected for the contribution of the gel capsule and for the core diamagnetism (using Pascal's constants). Field-dependent measurements were performed with H up to 50000 Oe on powder as well as a single crystal (0.3 mg). AC susceptibility measurements were performed on an aligned crystal weighing 3.4 mg. An oscillating field of 3 Oe was applied.

Received: March 29, 2007
Published online: June 14, 2007

Keywords: geometric frustration · iron · magnetic properties · magnetization steps · phosphates

[1] a) M. N. Leuenberger, D. Loss, *Nature* **2001**, *410*, 789 – 793; b) F. Meier, J. Levy, D. Loss, *Phys. Rev. B* **2003**, *68*, 134417.
[2] R. Sessoli, D. Gatteschi, A. Caneschi, M. A. Novak, *Nature* **1993**, *365*, 141 – 143.
[3] a) S.-J. Hwu, *Chem. Mater.* **1998**, *10*, 2846 – 2859; b) M. Ulutagay-Kartin, K. M. S. G. Etheredge, G. L. Schimek, S.-J. Hwu, *J. Alloys Compd.* **2002**, *338*, 80 – 86; c) S.-J. Hwu, M. Ulutagay-Kartin, J. A. Clayhold, R. Mackay, T. A. Wardojo, C. J. O'Connor, M. Krawiec, *J. Am. Chem. Soc.* **2002**, *124*, 12404 – 12405; d) M. Ulutagay-Kartin, S.-J. Hwu, J. A. Clayhold, *Inorg. Chem.* **2003**, *42*, 2405 – 2409; e) X. Mo, K. M. S. Etheredge, S.-J. Hwu, Q. Huang, *Inorg. Chem.* **2006**, *45*, 3478 – 3480; f) K. G. Sanjaya Ranmohotti, X. Mo, M. K. Smith, S.-J. Hwu, *Inorg. Chem.* **2006**, *45*, 3665 – 3670.
[4] See, for example: a) M. Murugesu, J. Raftery, W. Wernsdorfer, G. Christou, E. K. Brechin, *Inorg. Chem.* **2004**, *43*, 4203 – 4209, and references therein; b) L. K. Thompson, O. Waldmann, Z. Xu, *Coord. Chem. Rev.* **2005**, *249*, 2677 – 2690.
[5] S. K. Ritter, *Chem. Eng. News* **2004**, *82*(50), 29 – 32, and references therein.
[6] a) J. Snyder, B. G. Ueland, J. S. Slusky, H. Karunadasa, R. J. Cava, A. Mizel, P. Schiffer, *Phys. Rev. Lett.* **2003**, *91*, 107201; b) G. Ehlers, A. L. Cornelius, M. Orendac, M. Kajnakova, T. Fennell, S. T. Bramwell, J. S. Gardner, *J. Phys. Condens. Matter* **2003**, *15*, L9 – L15.
[7] a) A. Maignan, V. Hardy, S. Hébert, M. Drillon, M. R. Lees, O. Petrenko, D. M. Paul, D. Khomskii, *J. Mater. Chem.* **2004**, *14*, 1231 – 1236; b) V. Hardy, M. R. Lees, O. A. Petrenko, D. M. Paul, D. Flahaut, S. Hébert, A. Maignan, *Phys. Rev. B* **2004**, *70*, 064424.
[8] a) J. E. Greedan, *J. Mater. Chem.* **2001**, *11*, 37 – 53, and references therein; b) J. E. Greedan, *J. Alloys Compd.* **2006**, *408–412*, 444 – 455.
[9] a) S. Rosenkranz, A. P. Ramirez, A. Hayashi, R. J. Cava, R. Siddharthan, B. S. Shastry, *J. Appl. Phys.* **2000**, *87*, 5914 – 5916; b) D. Dai, M.-H. Whangbo, *Inorg. Chem.* **2005**, *44*, 4407 – 4414.
[10] a) D. S. Rana, S. K. Malik, *Phys. Rev. B* **2006**, *74*, 052407; b) J. C. Fernandes, F. S. Sarrat, R. B. Guimarães, R. S. Freitas, M. A. Continentino, A. C. Doriguetto, Y. P. Mascarenhas, J. Ellena, E. E. Castellano, J.-L. Tholence, J. Dumas, L. Ghivelder, *Phys. Rev. B* **2003**, *67*, 104413; c) A. Oiwa, A. Endo, S. Katsumoto, Y. Iye, H. Munekata, *Phys. Condens. Matter* **2000**, *284–288*, 1173 – 1174.
[11] R. D. Shannon, *Acta Crystallogr. Sect. A.* **1976**, *32*, 751 – 767.
[12] G. Becht, S.-J. Hwu, *Chem. Mater.* **2006**, *18*, 4221 – 4223.
[13] F. E. Mabbs, D. J. Machin, *Magnetism and Transition Metal Complexes*, Halsted Press, New York, **1973**.
[14] R. S. Drago, *Physical Methods in Chemistry*, W. B. Saunders, Philadelphia, **1977**.
[15] V. Hardy, D. Flahaut, M. R. Lees, Q. A. Petrenko, *Phys. Rev. B* **2004**, *70*, 214439.
[16] a) Q. Hung, S.-J. Hwu, unpublished results; b) M. B. Korzenski, G. L. Schimek, J. W. Kolis, G. J. Long, *J. Solid State Chem.* **1998**, *139*, 152 – 160.
[17] O. V. Yakubovich, O. K. Mel'nikov, V. S. Urusov, V. Massa, S. Vochadlo, *Dokl. Akad. Nauk* **1996**, *348*, 755 – 758.

